Dimensions Effect of the Rotating Fluid Zone on the Results when CFD Modeling of Friction Stir Welding

Esam Hamza*

emh6141@yahoo.com

Authority of Natural Science Research and Technology, Tripoli, Libya

ABSTRACT

This study aims to investigate the influence of the shape and size of rotating fluid region on the results of computational fluid dynamic (CFD) model of friction stir welding (FSW). Accordingly, 3D time-dependent CFD based model was used to simulate friction stir welding of aluminum alloy AA2014-T6. A rotating fluid region was proposed to represent the Thermo-mechanical affected zone (TMAZ) in the model where the temperature distribution within the materials being welded together has been critically analysed. By using different shapes and dimensions for the fluid region, a number of numerical experiments has been carried out. The results revealed that the thermal profile for the circular zone indicates the best agreement among the other with the experimental thermal profile. Additionally, a semi-empirical equation was developed to calculate the maximum temperature based on the dimensions of TMAZ.

Keywords: Friction Stir Welding (FSW), Computational Fluid Dynamics (CFD), Thermo-mechanical Affected Zone (TMAZ).

1 Introduction

Friction Stir Welding (FSW) was developed by Wayne Thomas et al at The Welding Institute (TWI) in The United Kingdom in 1991[1]. This welding process overcomes many of the problems associated with traditional joining techniques. FSW is applied in different field of industry due to its advantages such as high quality, the welding temperature does not exceed the melting point and shielding gas is not required. Furthermore, it's an effective alternative to weld dissimilar materials [2].

As a solid-state welding process, Friction Stir Welding (FSW) is carried out using a non-consumable, rotating and translating tool that is brought at the interface between the two work pieces to be welded. The heat generation leads to increase the temperature of the surfaces being welded in the near-tool region, which makes them soft. Then, the tool movement and its high mechanical pressure melds and joins both materials together.

For the purpose of understanding the physical phenomena associated with FSW particularly those are represented in the thermomechanical interrelations, several computational fluid dynamics (CFD) tool-based studies have been conducted. For simplification purpose, assumptions and different modelling techniques have been adopted particularly those related to defining the fluid region which represents thermo-mechanical affected zone (TMAZ) that taking place in the workpiece around the welding tool. However, the change in the proposed shape and size of the fluid region may affect the model accuracy.

The earlier works to CFD modelling of FSW have been mostly carried out in two-dimensions [3, 4]. However, P. A. Colegrove [5] have published a critical review of modelling of FSW which revealed that one of the most important issues is the development and validation of robust 3-dimensional model. After that, P. A. Colegrove and Shercliff [6] described the application of (CFD) code in modelling of friction stir welding. In their work, CFD package FLUENT 15.0 was used to build a 3-dimensional steady-state model which includes five regions. Firstly, a rotating zone represents the fluid region nearby the tool and moves at its rotational speed. Secondly, a slightly wider strip surrounds the rotating zone and extending to the length of the workpiece which represents the material flow at the tool travelling speed. The rest of the workpiece in both sides is modelled as solid aluminium regions to simulate the thermal response far away from the deformation zone. Finally, to calculate the heat losses to the tool and backing plate both of them were defined as solid regions. The results have

demonstrated that the CFD package, Fluent can be used to analyse the heat and material flow in FSW. However, the study has not shown the effect of the change in rotating zone dimensions as the size of the deformation zone in the model was larger than that recorded in the experimental work.

The 3-dimensional CFD model developed by S.Z Aljoaba et al [7] consisted two regions. Firstly, the tool which is assumed to be a solid body. Secondly, the workpiece which is assumed to be a fluid region. Although, the model has been validated with experimental data the rotating zone concept was not considered and temperature at the sides of the workpiece were kept fixed at room temperature.

The work published by Atharifar et al [8] used Fluent to solve the governing equations in the computational domain. In order to simplify the calculation time, a cylindrical computation zone was assumed with a diameter twice the diameter of the tool shoulder and rotates at the tool speed. This cylindrical fluid region is small compared to the actual size of the workpiece. The numerical results were found in a good agreement with the experimental data. However, the study has not given any information about the effect of the shape and size of the computation domain on the results.

Z. Zhang et al [9] have published a study includes an investigation of the effect of shoulder size on the temperature distributions and the material deformations in FSW. The workpiece was represented in the model used by a rounded zone with 80 mm diameter. The welding speed has been applied in the inflow region while the tool was considered to be a rigid body.

A 3-D transient CFD model was developed by ZHENZHEN YU et al [10] where the tool rotational motion was defined by giving the speed to a rotating zone which surrounds the tool. The authors used this model to investigate the influence of the pin thread on the thermal distribution and the material flow behaviour.

In the work carried out by S. Kang et al [2] the rotation affected zone RAZ concept was used in the computational domain of the model where the momentum and energy equations were solved using the CFD program Fluent. In the model used, RAZ represents the thermo-mechanically affected Zone TMAZ in real FSW process where the material plastic deformation occurs. The size of RAZ has determined in terms of dimensional variables a and b where a parametric study was carried out for various ranges of a and b to exactly define the RAZ. Consequently, the thermal analysis has shown when the value of a is 1mm and b is 2-3mm the temperature results have given the best agreement with the reference data. However, the study has been conducted in steady state condition and did not include the effect of the change in RAZ shape. Furthermore, the fluid zone proposed in the model developed is still big which includes the inflow and outflow region as well as the RAZ.

In advanced step to improve the transient CFD modelling of FSW, E. Hamza et al [11] has rotated a circular conical zone around the tool. The translational motion of the tool has been simulated by using the dynamic mesh while sliding mesh technique was employed to mimic the rotational movement. As the model was validated with experimental data, influence of the tool pin size on the temperature distribution has been investigated.

The majority of the published works presented above have not focused on the effect of the proposed rotational zone on the modelling results particularly in the transient analysis conditions. Hence, the current study is an extension of the works conducted by S. Kang and E. Hamza [2, 11], where different shapes and sizes for TMAZ are proposed and their effects on the thermal cycle of FSW will be studied. Consequently, a dimensionless formula will be developed to describe the relationship between the temperature and TMAZ dimensions. The model that will be used was constructed using the CFD commercial program Fluent 16.0.

2 Numerical Modelling

The 3-D CFD transient model used in this study was developed and validated by E. Hamza [11] where the computational domain that is shown in Figure 1 consists of two regions. The first region represents the thermo-mechanical affected zone (TMAZ) around the tool. This zone is treated as a fluid region which has a radial and conical shape, where its dimensions are based on design variables a and b as displayed in Figure 2 [2]. The tool pin has a conical triangular profile with a length of 4.7mm, where the pin side lengths at the root and the tip of the pin are 5.19mm and 3.11mm respectively. The shoulder has a constant diameter of 12mm. The dimensions of the plates to be welded are 300mm x 100mm x 5mm.

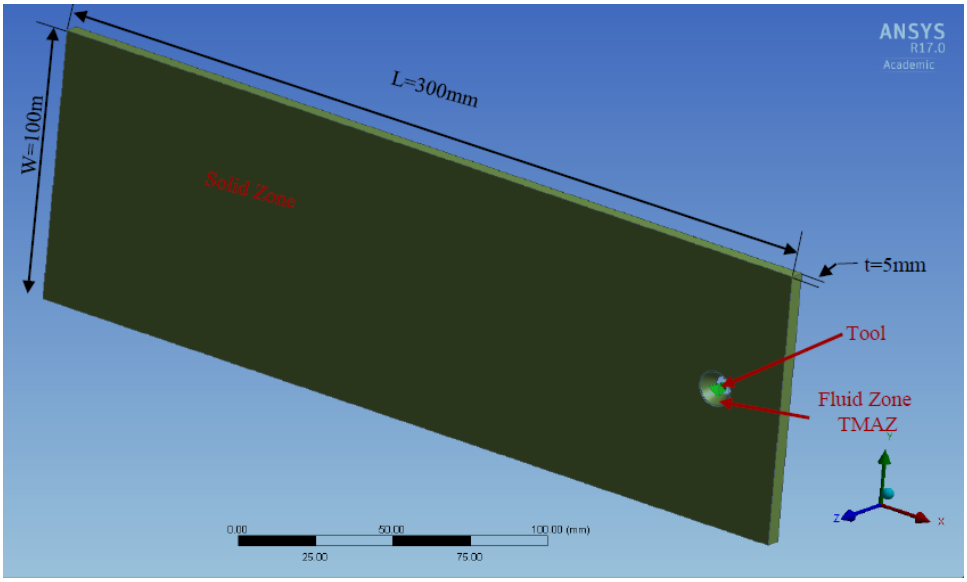

Figure 1: *Model Geometry*

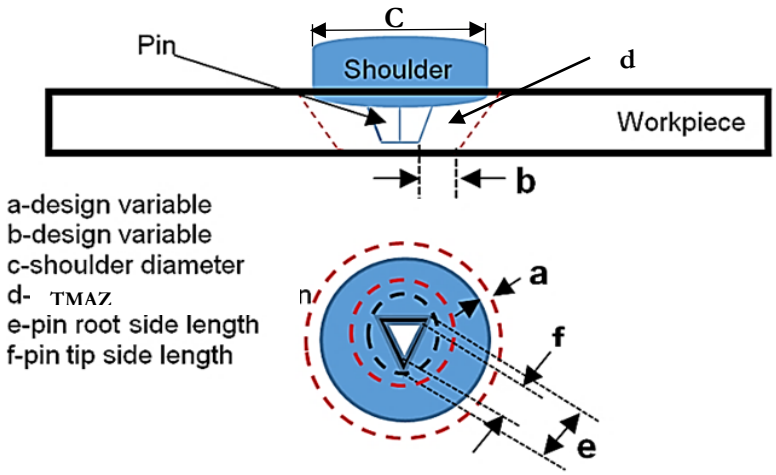

Figure 2: *Details of the Computational Domain*

Figure 3 shows the meshing of the computational domain where a new methodology was considered in which the translation motion of the tool has been specified using dynamic mesh technique, and considering the path followed by the tool as a solid region rather than fluid. As the temperature and velocity are steeply gradient in the (TMAZ), it has been finely meshed to capture this level of gradient whereas the rotation of the tool has been specified using sliding mesh technique. Due to configurations, tetrahedral elements were used for both the fluid and the solid regions. With a view to simulate FSW, the boundary conditions have been defined where the tool was specified with rotational and travel speeds of 1000rpm 7.73mm/s, respectively. User Defined Function (UDF) subroutine has been used in applying of the travel speed. Thermally, to define the process of heat generation, a heat flux was applied to the tool surface after it had been calculated by the analytical heat generation equation given as GADAKH [13]

$$Q = \frac{2}{3}\,\pi\mu\omega P\left(R^3_{Shoulder} + \frac{9}{4\pi}\,R^2_{prob}\,H_{prob}\right) \quad (1)$$

where, μ is the friction coefficient taken as 0.5, ω is the rotational speed of the tool, P is the plunging pressure which was kept at 90Mpa. During the heat transfer analysis, the convection heat transfer coefficient from the top and side surfaces of

the workpiece are 25W/m2 °C, and whereas the bottom surface is supported by a backing plate, the coefficient value is considered to be 200W/m2 °C. Kang [2].

.

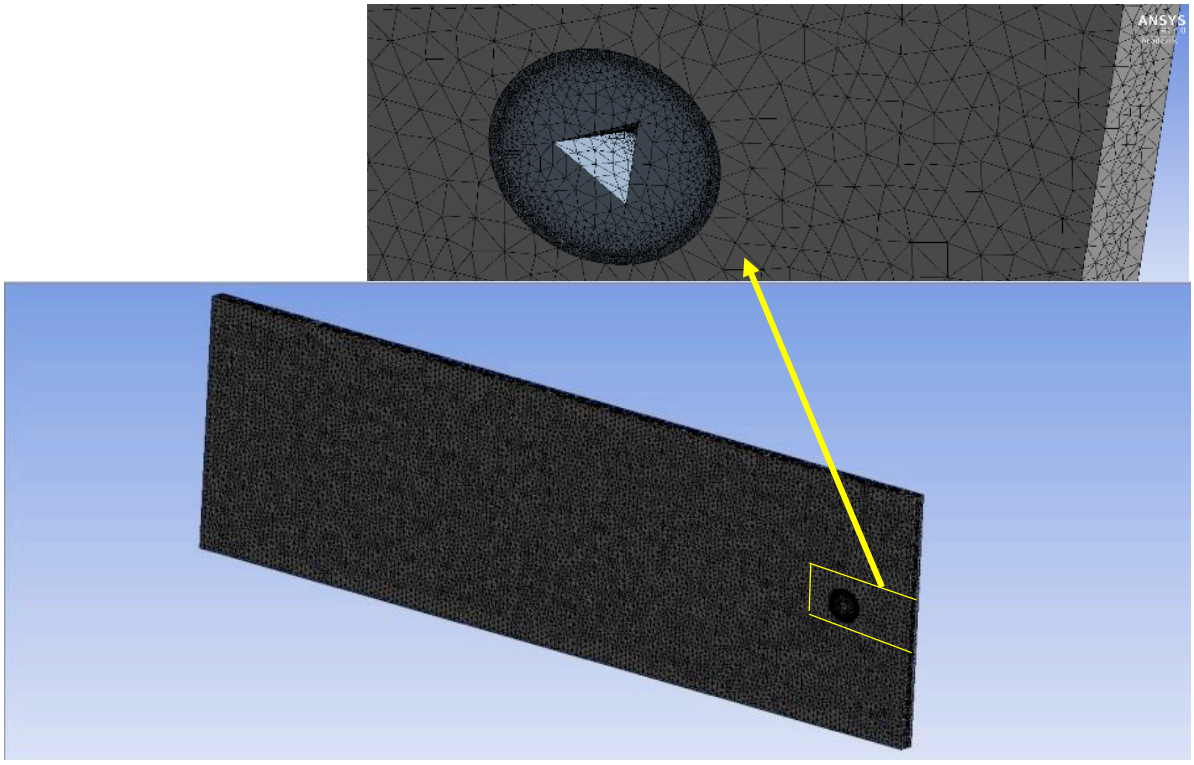

Figure 3: *Meshing of the Computational Domain*

Due to the resultant heat generation from the rotational speed of the tool, the material behaves as non-Newtonian viscoplastic fluid in the near tool region, with laminar flow conditions. The fluid flow is governed by mass and momentum conservation equations, whereas, in order to specify the conductive and convective heat transfer rates, the energy conservation equation is also employed. These equations can be found in many published literatures such as by Arora [12]. By using the Finite Volume Method (FVM), these governing equations for 3D transient heat transfer and fluid flow are discretized and solved iteratively during 6 seconds which are the welding time. More information about the model such as the material properties of the aluminium alloy AA2014-T6 are provided in the literature [2, 11, 14].

3 Investigating the effect of fluid zone (TMAZ) shape on the welding thermal cycle

In order to investigate the effect of the fluid region (TMAZ) shape in the current model, circular conical zone was proposed at the beginning with design variables a = 1mm and b = 2.5mm [2]. Then, in terms of a and b, the rear half of the zone has been changed by adding certain values for a and b where the region has got semi elliptical shapes. The reason behind that is just to examine the effectiveness of zone shape at the rear half in which the fluid zone shape and size are expected to be bigger than in the circular one as there is more hot metal accumulation in the trailing side than in the leading side. Figure 4 illustrates the fluid zone with different shapes. For conducting the study, six experiments have been designed with different shapes around a tool with a triangle pin as shown in table 1. As the model used in the current study has already been validated [11] and to study the effect of shape and dimensions of the fluid zone (TMAZ), the thermal cycles were monitored in all of proposed numerical experiments at a point with a distance 4mm from the weld centre, and a depth of 2mm from the top surface of the plates.

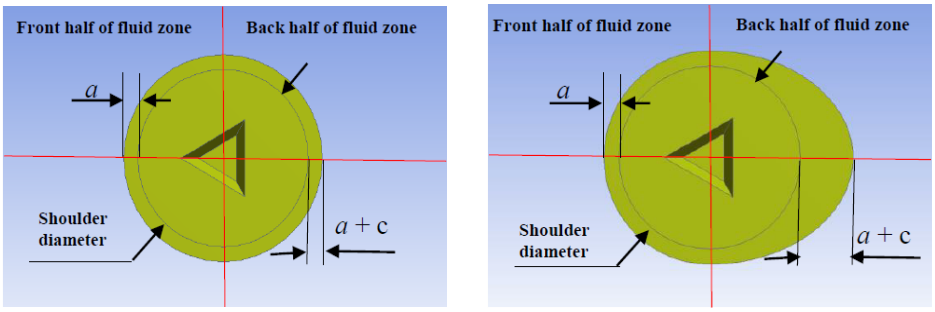

Figure 4: *conical circular and conical semi elliptical fluid zones.*

Table 1: *different shapes of fluid zones*

Experiment	Zone shape	Design variables(mm)	*c*(mm)	*a*+*c*(mm)	*b*+*c*(mm)
Ex.1	circular	*a*=1 , *b*=2.5	0	1	2.5
Ex.2	semi elliptical	*a*=1 , *b*=2.5	1	2	3.5
Ex.3	semi elliptical	*a*=1 , *b*=2.5	1.5	2.5	4
Ex.4	semi elliptical	*a*=1 , *b*=2.5	2	3	4.5
Ex.5	semi elliptical	*a*=1 , *b*=2.5	2.5	3.5	5
Ex.6	semi elliptical	*a*=1 , *b*=2.5	3	4	5.5

4 Investigating the effect of fluid zone (TMAZ) dimensions on the welding thermal cycle

The circular conical shape of the fluid zone (TMAZ) has been chosen to carry out this analysis whereas several values for design variables *a* and *b* were proposed. Based on the proposed values of *a* and *b*, fifteen different sizes of TMAZ were used in the numerical experiments as shown in table 2. In order to monitor the thermal cycle, the time dependent temperature profile was recorded for all proposed numerical experiments at a point with a distance 4mm from the weld centre, and a depth of 2mm from the top surface of the plates. As well known, the maximum temperature is one of the significant thermal features that has an important role in defining the final microstructure of the welded joint and its properties as well which in role estimate the final weld quality. Therefore, the maximum global temperature T*g, max* was monitored and recorded for each value of *a* and *b*. After conducting the set of experiments that have been designed based on different fluid zone dimensions and using a tool with the triangular pin, a relationship between the temperature ratio, design variables and the shoulder radius is expressed using multiple variable regression analysis.

Table 2: *different sizes of fluid zone*

Experiments No.	Value of *a* (mm)	Value of *b* (mm)
Ex.1	0.5	0.5
Ex.2	0.5	1.5
Ex.3	0.5	2.5
Ex.4	0.5	3.5
Ex.5	0.5	4.5
Ex.6	1	0.5
Ex.7	1	1.5
Ex.8	1	2.5
Ex.9	1	3.5
Ex.10	1	4.5

Ex.11	1.5	0.5
Ex.12	1.5	1.5
Ex.13	1.5	2.5
Ex.14	1.5	3.5
Ex.15	1.5	4.5

5 Results and discussion

As the numerical experiments shown in table 1 have been conducted for different shapes of TMAZ, what can be seen in Figure 5 is the thermal cycles for those simulated welding processes. The thermal profile of TMAZ with *a*=1mm and *b*=2.5mm (the circular conical zone) indicates the best agreement among the other with the experimental thermal profile. By considering the maximum temperature of the best CFD thermal profile, one can notify that there is no much difference compared to the maximum temperature of the other calculated thermal profiles. However, the cooling rate becomes faster when using the semi elliptical shape of TMAZ rather than the circular one. It would be said that the heat dissipation between the fluid zone and the solid zone is enhanced as long as the heat transfer area is increased due to increase in the fluid zone dimensions. For more explanation, the static temperature distribution has been depicted in Figure 6. It can be seen that the temperature is higher on the advancing side than on the retreating side, which is due to the opposite direction of the material flow on the advancing region to that of the tool motion.

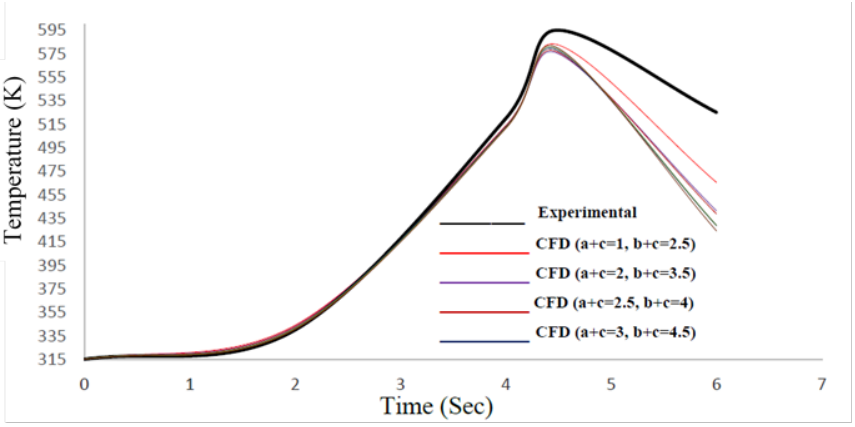

Figure 5: *comparison between different thermal cycles for different TMAZ shapes corresponding measured thermal cycle*

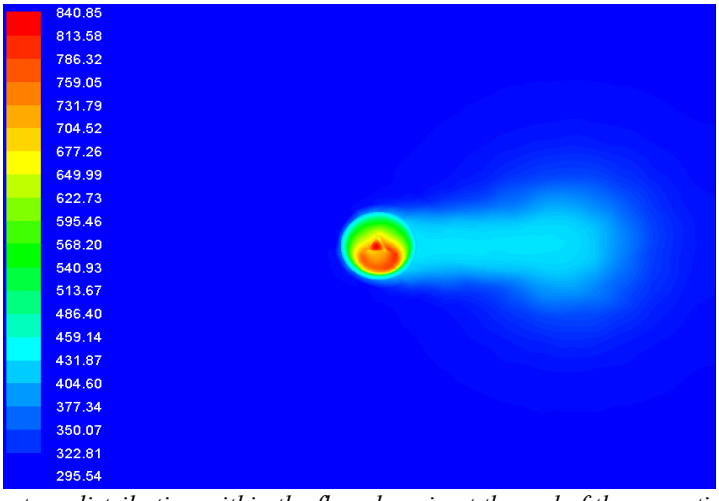

Figure 6: *Temperature distribution within the flow domain at the end of the operational cycle*

Based on the results recorded in section 3, the circular conical shape of TMAZ has been considered to conduct the analysis in the current section. Figures 7, 8 and 9 exhibit the comparison between different thermal cycles for different values of *a* and *b*. Looking at these figures and considering the temperature trend with time, maximum temperatures and cooling rates, it can be found that some values of the maximum temperature exceed the corresponding measured values. Those values are not physically accepted in terms of fact of the maximum temperature should not exceeds the experimental value for the same due to ignoring the part of heat generation from material deformation. Accordingly, the thermal profile of *b*=2.5mm (blue curve) for the three values of *a* has in general the best agreement with the experimental data among the other profiles in the same set of experiments. However, by drawing an analogy between the best three profiles; the one with *a* =1mm and *b*=2.5mm depicts the optimum behaviour based on the three mentioned thermal features. Consequently, this is an approval in a transient state for the work done by Kang et al. [2] who has used a steady state CFD model in finding the optimum values for *a* and *b* which are 1mm and 2.5mm respectively.

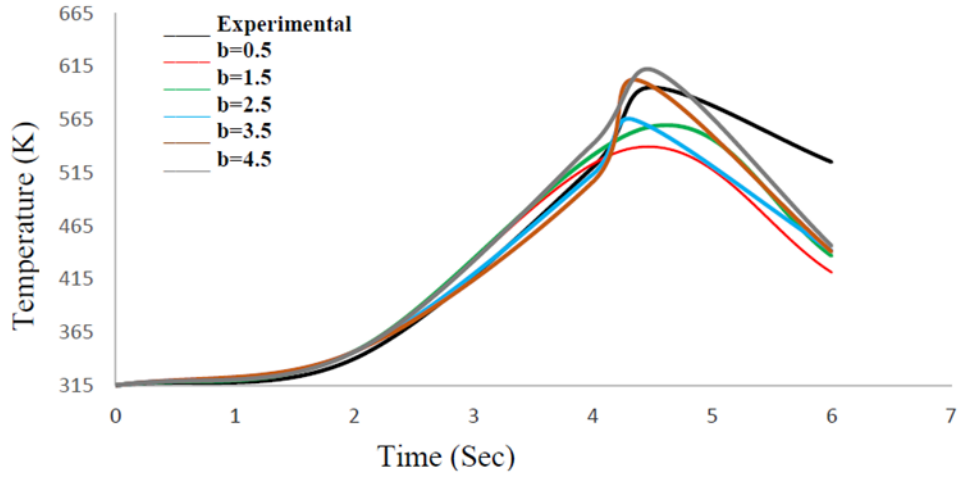

Figure 7: *a comparison between different thermal cycles for different values of b when a=0.5*

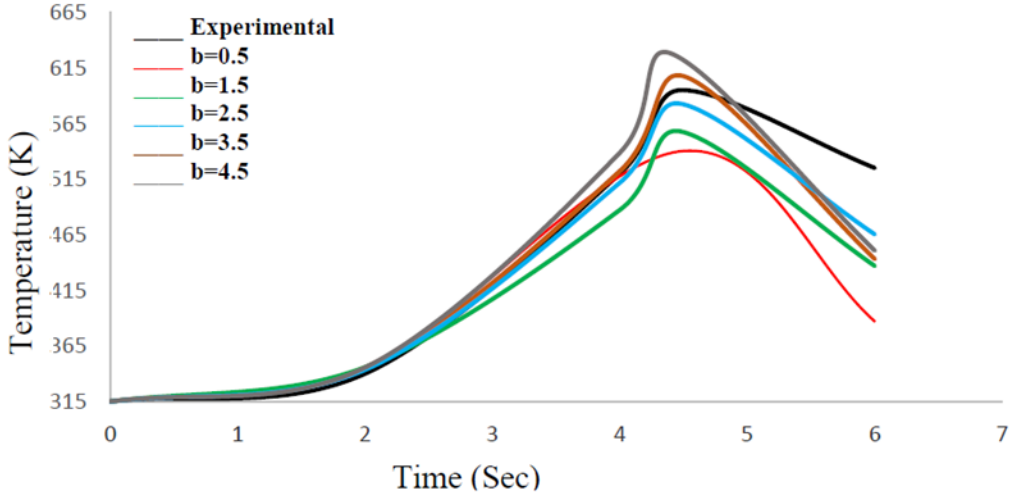

Figure 8: *a comparison between different thermal cycles for different values of b when a=1*

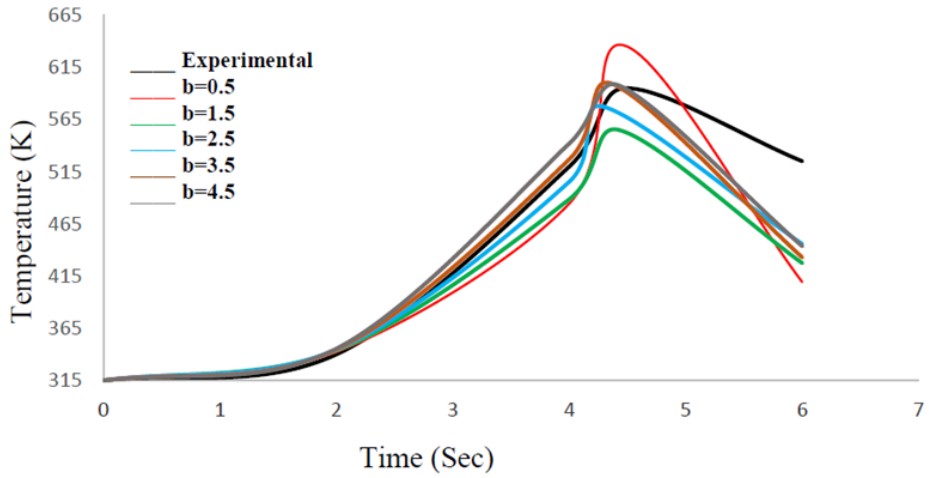

Figure 9: *a comparison between different thermal cycles for different values of b when a=1.5*

Table 3 presents the recorded values of T*g, max* against the values of *a* and *b* in the fifteen numerical experiments. Noticeably, a proportional relationship between the values of *b* and T*g, max* is taking place, where the increasing in *b* is met by an increasing in T*g, max*. Beside the absence of heat amount due to the plastic deformation, the quantity of fluid mass increases according to the increase in *b* which leads to less volume change compared to *a* [2]. Therefore, the heat resistance becomes higher as the outer fluid particles experiences decreasing in their kinetic energy which allow the temperature to be risen up.

Table 3: *the computed values of Tg, max according to different values of a and b*

a=0.5 (mm)		*a*=1(mm)		*a*=1.5	
b (mm)	T*g, max*	*b* (mm)	T*g, max*	*b* (mm)	T*g, max*
0.5	735	0.5	720	0.5	726
1.5	743	1.5	734	1.5	734
2.5	760	2.5	780	2.5	760
3.5	790	3.5	799	3.5	777
4.5	796	4.5	799	4.5	798

Based on the data from CFD experiments with the aid of multiple variable regression analysis, a dimensionless formula can be developed to describe the relationship between the temperature ratio T*g, max* / (T*g, max* - T*in*) and geometrical variables *a*, *b*, and the shoulder radius Rs.

$$\frac{T_{g,max}}{T_{g,max} - T_{in}} = \frac{1.66\left(\frac{a}{R_s}\right)^{0.0044}}{\left(\frac{b}{R_s}\right)^{0.0311}} \qquad (2)$$

where T*in* is the initial temperature which is equal to 315°K. Then, Equation (2) can be modified to find a direct expression to calculate T*g, max* as following:

$$T_{g,max} = -\left[\frac{\frac{1.66\left(\frac{a}{R_s}\right)^{0.0044}}{\left(\frac{b}{R_s}\right)^{0.0311}}}{1-\frac{1.66\left(\frac{a}{R_s}\right)^{0.0044}}{\left(\frac{b}{R_s}\right)^{0.0311}}}\right] \times T_{in} \quad (3)$$

It is observed that *b* has a greater effect on T*g, max* than *a*. In order to authorise the utility of equation (3), the difference between the T*g, max* values from equation (3) and the CFD T*g, max* values, both of them were plotted in Figure 10. Obviously, within the ±5 error bounded of the developed equation it would be seen that 100% of the data lies in this range. Therefore, Equation 3 can be used to determine the maximum temperature with reasonable accuracy [15] particularly; the current study would be experimentally and analytically difficult so far. Last but not least, the above expressed equation is valid for Rs=6mm.

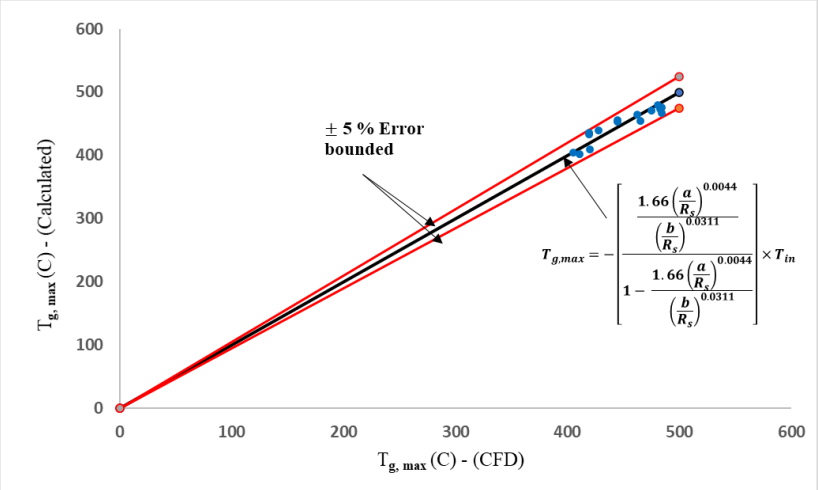

Figure 10: *a comparison between the maximum temperature computed by the developed equation and that CFD estimated*

6 Conclusion

In this work, heat transfer analysis is carried out using the CFD commercial program 'Fluent 17.0'. In order to achieve the objectives defined for the current study, a number of numerical experiments were carried out. When examining the effect of TMAZ shape on the welding thermal features, the thermal profile of TMAZ with *a*=1mm and *b*=2.5mm (the circular conical zone) indicates the best agreement among the other with the experimental thermal profile. Additionally, the cooling rate becomes faster when using the semi elliptical shape of TMAZ rather than the circular one.

Similarly, when analysing the effect of TMAZ dimensions on the thermal features, the thermal profile of *b*=2.5mm for the three values of *a* has in general the best agreement with the experimental data among the other profiles in the same set of experiments. Inspite of that, and between the best three profiles, the one with *a*=1mm and *b*=2.5mm depicts the optimum behaviour. Moreover, the developed equation based on multiple variable regression analysis has revealed that T*g, max* is greater influenced by *b* than *a* and the usefulness of this formula has been authorised where within ±5 error bounded of the developed equation; 100% of the data lies in this range. Finally, this work can be extended by considering other operational and geometrical variables.

References

[1] W. Thomas, et al, "Friction stir butt welding Int Patent App PCT/GB92/02203, and GB Patent App 9125978.8," *US Patent*, vol. 5, pp. 317-460, December 1991.

[2] S.W. Kang, et al, "A study on heat-flow analysis of friction stir welding on a rotation affected zone," *Journal of mechanical science and technology*, vol. 28, no.9, pp. 3873-3883, 2014. https://doi.org/10.1007/s12206-014-0851-6.

[3] X. Deng, et al, "Two-dimensional finite element simulation of material flow in the friction stir welding process," *Journal of manufacturing processes*, vol. 6, no. 2, pp. 125-133, 2004. https://doi.org/10.1016/S1526-6125(04).

[4] T. Seidel, et al, "Two-dimensional friction stir welding process model based on fluid mechanics," *Science and technology of welding and joining*, vol. 8, no. 3, pp. 175-183, 2003. https://doi.org/ DOI 10.1179/136217103225010952.

[5] P. A. Colegrove, "Modelling of friction stir welding," *Doctoral Thesis*, Cambridge University, 2004. https://doi.org/10.17863/CAM.14008.

[6] P. A. Colegrove, et al, "3-Dimensional CFD modelling of flow round a threaded friction stir welding tool profile," *Journal of Materials Processing Technology*, vol. 169, no. 2, pp. 320-327, 2014. https://doi.org/10.1016/j.jmatprotec

[7] S. Aljoaba, et al, "Modeling of friction stir processing using 3D CFD analysis," *International journal of material forming*, vol. 2, no. 1, pp. 315-318, 2009. https://doi.org/10.1007/s12289-009-0662-y.

[8] H. Atharifar, et al, "Numerical and experimental investigations on the loads carried by the tool during friction stir welding," Journal *of Materials ngineering and Performance*, vol. 18, no. 4, pp. 339-350, JMEPEG, 2009. https://doi.org/10.1007/s11665-008-9298-1.

[9] Z. Zhang, et al, "Effect of shoulder size on the temperature rise and the material deformation in friction stir welding," *The International Journal of Advanced Manufacturing Technology*, vol. 45, no. 9, pp. 889-895, Int J Adv Manuf Technol, 2009. https://doi.org/10.1007/s00170-009-2034-7.

[10] Yu. Zhenzhen, et al, "Transient heat and material flow modeling of friction stir processing of magnesium alloy using threaded tool," *Metallurgical and Materials Transactions A*, vol. 43, no. 2, pp. 724-737, 2012. https://doi.org/10.1007/s11661-011-0862-1.

[11] E. Hamza, et al, "Computational Fluid Dynamics based Transient Thermal Analysis of Friction Stir Welding," *6th International and 43rd National Conference on Fluid Mechanics and Fluid Power*, December, 2016. http://eprints.hud.ac.uk/id/eprint/29395/1/Esam.pdf.

[12] A.Arora, et al, "Strains and strain rates during friction stir welding," *Scripta Materialia*, vol. 61, no. 9, pp. 863-866, 2009. https://doi.org/10.1016/j.scriptamat.2009.07.01.

[13] V. Gadakh, et al, "Analytical modeling of the friction stir welding process using different pin profiles," *Welding Journal*, vol. 94, no. 4, pp. 115-124, 2015.

[14] M. Mehta, et al, "Numerical modelling of friction stir welding using the tools with polygonal pins*," Defence Technology*, vol. 11, no. 3, pp. 229-236, 2015.

[15] T. Asim, et al, "CFD based investigations for the design of severe service control valves used in energy," *Energy Conversion and Management*, vol. 153, pp. 288-303, 2017. https://doi.org/10.1016/j.enconman.2017.10.012.